Open access • Journal Article • DOI:10.1038/NM.4466

High-dimensional single-cell analysis predicts response to anti-PD-1 immunotherapy — Source link

Carsten Krieg, Malgorzata Nowicka, Malgorzata Nowicka, Silvia Guglietta ...+9 more authors

Institutions: University of Zurich, Swiss Institute of Bioinformatics, European Institute of Oncology

Published on: 08 Jan 2018 - Nature Medicine (Nature Publishing Group)

Topics: Immunotherapy, Melanoma, Mass cytometry and Peripheral blood mononuclear cell

High-dimensional single-cell analysis predicts response to anti-PD-1 immunotherapy

Krieg, Carsten ; Nowicka, Malgorzata ; Guglietta, Silvia ; Schindler, Sabrina ; Hartmann, Felix J ; Weber, Lukas M ; Dummer, Reinhard ; Robinson, Mark D ; Levesque, Mitchell P ; Becher, Burkhard

Abstract: Immune-checkpoint blockade has revolutionized cancer therapy. In particular, inhibition of programmed cell death protein 1 (PD-1) has been found to be effective for the treatment of metastatic melanoma and other cancers. Despite a dramatic increase in progression-free survival, a large proportion of patients do not show durable responses. Therefore, predictive biomarkers of a clinical response are urgently needed. Here we used high-dimensional single-cell mass cytometry and a bioinformatics pipeline for the in-depth characterization of the immune cell subsets in the peripheral blood of patients with stage IV melanoma before and after 12 weeks of anti-PD-1 immunotherapy. During therapy, we observed a clear response to immunotherapy in the T cell compartment. However, before commencing therapy, a strong predictor of progression-free and overall survival in response to anti-PD-1 immunotherapy was the frequency of CD14+CD16−HLA-DRhi monocytes. We confirmed this by conventional flow cytometry in an independent, blinded validation cohort, and we propose that the frequency of monocytes in PBMCs may serve in clinical decision support.

DOI: https://doi.org/10.1038/nm.4466

Title: High dimensional single cell analysis predicts response to anti-PD-1 immunotherapy

Authors: Carsten Krieg*[1], Malgorzata Nowicka[2,3], Silvia Guglietta[4], Sabrina Schindler[5], Felix J. Hartmann[1], Lukas M. Weber[2,3], Reinhard Dummer[5], Mark D. Robinson[2,3], Mitchell P. Levesque[#*5], Burkhard Becher[#*1].

Affiliations:

[1]Institute of Experimental Immunology, University of Zurich, Winterthurerstr. 190, 8057 Zurich, Switzerland

[2]Institute of Molecular Life Sciences, University of Zurich, Winterthurerstr. 190, CH-8057 Zurich, Switzerland

[3]SIB Swiss Institute of Bioinformatics, University of Zurich, Winterthurerstr. 190, CH-8057 Zurich, Switzerland

[4]Department of Experimental Oncology, European Institute of Oncology, Via Adamello 16, I-20139 Milan, Italy

[5]Department of Dermatology, University Hospital Zurich, CH-8091 Zurich, Switzerland.

***Correspondence to:** krieg@immunology.uzh.ch, mitchell.levesque@usz.ch or becher@immunology.uzh.ch

#these authors contributed equally

One sentence summary: The frequency of $CD14^{+}CD16^{-}HLA\text{-}DR^{hi}$ classical monocytes predicts response of melanoma patients to anti-PD-1 immunotherapy.

ABSTRACT

Immune checkpoint blockade has revolutionized cancer therapy. In particular, inhibition of programmed cell death protein 1 (PD-1) is effective for the treatment of metastatic melanoma and other cancers. Despite a dramatic increase in progression-free survival, a large proportion of patients do not show durable response. Therefore, predictive biomarkers of clinical response are desperately needed. Here, we employed high-dimensional single cell mass cytometry and a bioinformatics pipeline for the in-depth characterization of the immune compartment in liquid biopsies from the same metastatic melanoma patient before and after anti-PD-1 immunotherapy. We could observe a clear treatment response to immunotherapy in the T cell compartment. However, a strong predictor of progression free and overall survival in response to anti-PD-1 immunotherapy was the frequency of $CD14^{+}CD16^{-}HLA\text{-}DR^{hi}$ monocytes. We could confirm this by regular flow cytometry in an independent validation cohort and propose this as a novel predictive biomarker for therapy decisions in the clinic.

INTRODUCTION

Immunotherapy with anti-PD-1 aims to block the interaction of tumor-reactive T cells with PD-1 ligands (PD-L1 and PD-L2) expressed on various cell types including leukocytes and the tumor cells themselves[1]. Clinical trials on PD-1 and PD-L1 blockade for patients with advanced melanoma have demonstrated consistent therapeutic responses, thus prompting their application to several other cancers[2-8].

Despite these encouraging results, clinical outcomes remain highly variable, with only a fraction of patients showing durable responses, some with early progression and others with late response, while the majority of treated patients show no beneficial clinical response[2,9]. Reliable criteria to discriminate responders from non-responders prior to treatment initiation are urgently needed. Predictive biomarkers would allow for the selection of patients who are more likely to respond and to provide potential non-responders with alternative, perhaps more efficacious, therapeutic options. Some recent reports used single-cell analysis to evaluate the expression of PD-1 and downstream signaling molecules on tumor infiltrating and circulating $CD8^+$ T cells with the aim of identifying such predictive biomarkers[10,11]. However, these approaches are hampered by the limited accessibility of patient material, low dimensionality, overfitting due to the absence of independent validation cohorts, and lack of systematic, unbiased bioinformatics pipelines resulting in a paucity of predictive biomarkers to date[12]. Single-cell analysis of human immune compartments has so far been limited by the parameters that can be visualized by conventional flow cytometry[13].

In this study, we used peripheral blood mononuclear cells (PBMC) from metastatic melanoma patients before and during therapy as a readily accessible and minimally invasive biopsy that has been shown to be more representative than tumor biopsies to probe immune signatures associated with responsiveness to anti-PD-1 immunotherapy[14]. High dimensional, single cell mass cytometry was used along with optimized immune marker panels and a customized, interactive bioinformatics pipeline to generate a thorough analysis of the peripheral blood immune cells in an effort to identify a responsiveness-associated predictive signature.

RESULTS

Stratification of responders versus non-responders using single cell mass cytometry

We performed the initial analysis with 40 cryopreserved PBMC samples isolated from the blood of a cohort of 20 melanoma patients before and after anti-PD-1 immunotherapy, as well as 20 samples from 10 age- and sex-matched healthy donors (toal N=60). Baseline samples and samples obtained after 12 weeks of anti-PD1 therapy originated from the same patients (Table 1, Figure 1A and Supplementary Figure 17).

Table 1. Characteristics of blood samples from melanoma patients and healthy donors used for the biomarker discovery study.

		Before therapy	**After therapy**	**Total**
Healthy donors	N dataset 1	5	5	
	N dataset 2	5	5	
	N TOTAL	10	10	20
	Age in years – mean (range)	60.3 (46-71)		
	Sex – male/female	6/4		
Melanoma patients				
Responders	N dataset 1	5	5	
	N dataset 2	6	6	
	N TOTAL	11	11	22
	Age in years – mean (range)	62.0 (42-81)		
	Sex – male/female	9/2		
Non-responders	N dataset 1	5	5	
	N dataset 2	4	4	
	N TOTAL	9	9	18
	Age in years – mean (range)	57.8 (45-75)		
	Sex – male/female	5/4		

For the CyTOF analysis, frozen PBMCs were thawed and stained (Figure 1A and Supplementary Table 1) using three separate and partially overlapping mass cytometry panels, one for the phenotypic characterization of lymphocytes, one for T cell function and one specifically for the in-depth characterization of myeloid cells. The first staining panel contained 30 leukocyte markers to identify all major immune cell populations and cover all stages of T cell differentiation and activation (Supplementary Table 1). After acquisition, each sample was de-barcoded using Boolean gating. Staining quality was evaluated by defining a biological positive and negative control (Supplementary Figure 1).

After data pre-processing (see Methods), we performed hierarchical clustering on normalized (per batch) median marker expression values on $CD45^+$ live cells in every patient before and after therapy. As shown in Figure 1B, the dendrogram displayed two major clades of samples. The left branch contained 15 samples, of which all were responders, whereas the right branch consisted of 72% non-responders (18/25). Thus, normalized median marker expression was sufficient to robustly separate most responders from non-responders. The unbiased clustering approach stratified the patients into responders and non-responders prior to therapy, which encouraged us to analyze the dataset more deeply.

Altered T cell memory compartment before therapy in responders

We began our comparative analysis between responders and non-responders, before and after therapy initiation, by investigating the global (measured based on all the cells) median expression of the 29 markers (Figure 1C). Significant increases in the expression of HLA-DR, CTLA-4, CD56, and CD45RO and decreased amounts of CD3, CD27, and CD28 were observed in responders versus non-responders.

Next, we sought to identify which cell populations best described the cellular frequency differences between responders and non-responders. Markers used for subsequent cell clustering were selected using the PCA informativeness score established by Levine et al.[15], cells were clustered using the FlowSOM algorithm[16,17] with consensus clustering, separately for each of the measurements rounds. A two-dimensional t-stochastic neighbor embedding (tSNE) projection[18] was used for visualization along with heatmaps of normalized (0-1) median marker expression in each cluster, as shown in Figure 1D. Based on the median marker intensities observed in the clusters, we manually annotated the seven major cell populations (CD4 T cells, CD8 T cells, NK cells, NKT cells, B cells, γδT cells, and myeloid cells) in both measurement rounds. We subsequently examined differences in frequencies of the identified clusters between the three groups (HD, NR, R) (Figure 1E) using generalized mixed models (see workflow[19] and Supplementary Methods). Of note, the barcoding allowed the model to track the patients and match baseline and on-treatment samples for the analysis. In responders, the frequency of $CD4^+$ T cells and $CD8^+$ T cells was lower, while the frequency of CD19- HLA-DR+ myeloid cells was significantly elevated (adjusted p-values = 1.55e-05, 1.74e-03 and 1.74e-03, respectively) compared to the non-responders (before and during treatment, Figure 1E

and F). We also observed a higher frequency of NKT cells and a lower frequency of γδT cells (adjusted p-values = 3.07e-03 and 2.52e-03) in responders versus non-responders at both time points. In order to evaluate whether the immune status in the blood of responders might be reflected in the tumor environment, we analyzed 23 matched tumor biopsies within our cohort. Specifically, we assessed the infiltration by T cells (CD3, CD8, CD4), the number of phagocytes (CD68, CD163), as well as the expression of PD-L1. As expected, we found that responding patients had higher numbers of infiltrating $CD4^+$ T cells and $CD8^+$ T cells (Supplementary Figure 2).

Since T cells are described to be the major target of anti-PD-1 immunotherapy, and given the altered T cell composition in responders before immunotherapy, we next compared the median marker expression on $CD4^+$ and $CD8^+$ T cells (isolated *in silico* from the sets displaying in Figure 1D, 1E) between non-responders and responders before and after therapy. Global differential marker expression on merged samples in $CD4^+$ T cells in responders showed an up-regulation of CTLA-4, HLA-DR, CD69, and BTLA (Figure 2A). $CD8^+$ T cells in responders showed a higher expression of CD45RO, CTLA-4, CD62L, CD69, CD11a, and CCR4 (Figure 2B). This finding, together with the enrichment of $CD8^+$ T cells in the tumor biopsies of responding patients, suggests that their $CD8^+$ T cells show a higher migratory capacity.
To determine whether there were differences in T cell subpopulations, we reran FlowSOM on the extracted $CD4^+$ T cells and $CD8^+$ T cells and subdivided them into $CD45RO^-CD62L^+$ naïve, $CD45RO^-CD62L^-$ effector cells (TE), $CD45RO^+CD62L^-$ effector memory (EM) cells, $CD45RO^+CD62L^+$ central memory (CM) cells or $CD127^-CD25^+$ regulatory T cells (T_{regs}) by manual annotation[19].

We then compared the frequencies of resultant T cell sub-clusters between responders and non-responders before and 12 weeks after therapy (Figure 2C and 2D). The patients who eventually responded to the therapy showed a significantly lower frequency of circulating $CD4^+$ EM T cells, as well as a lower frequency of $CD8^+$ naïve T cell at baseline and after treatment (adjusted p-values = 8.21e-03, 6.95e-03, respectively). Additionally, the $CD8^+$ T cell subpopulation of responders had a higher frequency of CM T cells before and after treatment as compared to non-responder patients. In order to refine our analysis on $CD8^+$ T cells, which have previously been associated with response to anti-PD-1 immunotherapy[20,21], we analyzed the phenotype

of $CD8^+$ T cell clusters at higher resolution using 100 FlowSOM clusters before and after therapy (Supplementary Figure 3). Only 2 clusters were found to be differentially abundant before therapy while 10 clusters after therapy were expanded in responders, which clearly shows a therapy-induced proliferative burst. Cluster 16 ($CD45RO^+$, $CD27^+$, $HLA\text{-}DR^+$) closely resembles the central memory $CD8^+$ T cells, which were previously described to expand during anti-PD1 immunotherapy[20]. In agreement with previous research, we also found an increase in Tregs in cancer patients compared to healthy controls (Figure 2C).

Anti-PD-1 immunotherapy alters the properties within the T cell compartment

In order to compare the functional properties of T cells between non-responders and responders, we designed a second mass cytometry panel to investigate cytokine production (Supplementary Figure 4) in polyclonally activated cells. PBMCs were processed as described above. Briefly, single cell suspensions were cultured for 4h in the presence of PMA/Ionomycin, barcoded, stained, fixed and analyzed by mass cytometry. In order to analyze T cell function and the T cell phenotype independently, we first used surface markers (CD45RO, CD45RA, CCR7, CD28, CD127, CD69 and CD25) to define T cell subpopulations as in Figure 2C and 2D. Independent of the surface markers we extracted the frequencies of cytokine (IL-2, IL-4, IL-10, IL-13, IL-17A, GM-CSF, TNF-α, IFN-γ, Grz-B), PD-1 and CTLA-4 positive T cells. Importantly, we found a modest increase in IL-4, granzyme-B, IFN-γ, and GM-CSF in $CD4^+$ T cells and CTLA4, granzyme-B and IL-13 in $CD8^+$ T cells between responders and non-responders prior to therapy (data not shown). However, after therapy T cells from responders presented with higher frequencies for PD-1, IL-4, IFN-γ, IL-10, IL-17A, and granzyme-B in $CD4^+$ T cells (Figure 3A-D). For $CD8^+$ T cells, an up-regulation of CTLA4 and granzyme-B was detected in responders (Figure 3E-H). In order to account for multifunctional T cells, we created a binary matrix containing all possible cytokine and PD-1 and CTLA-4 presence / absence combinations (based on marker-specific cutoffs; see Supplementary Materials for further details) in $CD4^+$ T cells or $CD8^+$ T cells. Cytokine combination groups (CCG) that were found to be differentially abundant between responders and non-responders are displayed for $CD4^+$ T cells or $CD8^+$ T cells in Figure 3B and 3F, respectively. Using this approach, we found 3 CCGs in the $CD4^+$ T cell subsets that were observed

at a higher frequency in responders compared to non-responders (Figure 3C). For $CD8^+$ T cells, we found 13 CCGs that were expanded and 1 CCG that was reduced in responders (Figure 3G). The significantly different CCGs were then linked back and displayed in context to the initial T cell subpopulation. Among the enlarged CCGs in the $CD4^+$ T cells, the most common signature was CTLA-4^+, granzyme-B^+, TNF-α^+, and PD-1^+, thus the phenotype of these CCGs resembled CM (Figure 3D). As for the $CD8^+$ T cells, CCG 1, which was the only one down-regulated in frequency when comparing responders to non-responders, expressed no cytokines and its cell surface proteome resembled TE cells (Figure 3H). The only other cell population resembling TE cells was CCG 14, which was Granzyme-B^+, TNF-α^+, IFN-γ^+, and IL-2^+. The remaining 12 CCGs were expanded and were positive for at least two marker/cytokine combinations, thus most likely resembling so-called multifunctional T cells; all 12 were $CTLA4^+$ and displayed a CM/TM or EM surface phenotype (Figure 3H). $CTLA4^+$ CCGs could be separated into four groups distinguishable by their cytokine and CTLA4/PD-1 expression: CCGs 4, 5, 12, 13, 21, and 28 expressed CTLA4 and were granzyme-B^+, CCGs 44 and 45 were $CTLA4^+$, TNF-α^+, or IL-2^+, CCGs 22, 30; 36 were all CTLA4 positive and produced IL-2 or IL-17 and CCG 43 was only $CTLA4^+$. Surface phenotype and cytokine profiles of the previously identified CCGs overlap with previously published $CD45RA^-Grz\text{-}B^+CD8^+$ T cell populations expanding under anti-PD-1 immunotherapy[20,21].

Myeloid cell frequencies predict responsiveness to anti-PD-1 immunotherapy

Since we found higher frequencies of myeloid cells in anti-PD-1 therapy responders before therapy (Figure 1E), we interrogated a third myeloid centric panel (Supplementary Figure 5). FlowSOM was used to separate 7 subpopulations, which were annotated as T cells, B cells, NK cells, $CD14^+(CD11b^+HLA\text{-}DR^{hi})$ myeloid cells, $CD14^-(CD11b^+HLA\text{-}DR^{lo})$ myeloid cells, classical $CD1c^+CD11c^+HLA\text{-}DR^+$ dendritic cells cDC, and plasmacytoid dendritic cells ($CD123^+CD303^+HLA\text{-}DR^+CD11c^-$ pDC). For the annotated clusters, cell frequencies were calculated in each sample and the composition of the individual samples was plotted (Figure 4A and Supplementary Figure 6). As already shown in Figure 1D, a significant lower frequency of T cells (p-value = 1.59e-03) and a higher frequency of $CD14^+$ myeloid cells was observed in responders (p-value = 5.82e-03, Supplementary Figure 6). Next, to better characterize

the myeloid cells, we extracted live myeloid cells by manually gating out $CD3^+$ and $CD19^+$ cells, clustered, annotated and excluding $CD7^+$ and $CD56^+$ cells and marker expression from further analysis. Unsupervised clustering of normalized median marker expression values in myeloid cells again separated patients into two distinct clusters, with one clade being mostly composed of non-responders (12/14; 86%) and the other clade consisting of 76% (19/25) responders (Figure 4B). While we found that $CD14^-$ myeloid cells were indeed higher in cancer patients compared to healthy donors, we did not observe differences in this cell population between responders and non-responders.

We next searched for changes in global median marker expression between non-responders and responders, before and 12 weeks after therapy, and we found that 16 markers (i.e., CD86, HLA-DR, CD141, ICAM-1, CD11c, PD-L1, CD38, CD16, CD33, CD11b, CD303, CD62L, CD1c, CD64, CD14, and CD34) were significantly up-regulated in the myeloid compartment of responders (Figure 4C). Of note, the enhanced frequency of IFN-γ-producing T cells correlated with the expansion of the myeloid compartment and PD-L1 expression after therapy (Supplementary Figure 7). Next, FlowSOM was used to subdivide the myeloid compartment into 4 major clusters, which were annotated as $CD14^+CD16^-$HLA-DR^{hi} classical monocytes, $CD14^-CD33^{low}CD11b^+$HLA-DR^{lo} myeloid cells, plasmacytoid dendritic cells ($CD123^+CD303^+$HLA-DR^+CD11c^- pDC) and classical $CD1c^+CD11c^+$HLA-DR^+ dendritic cells (cDC, Figure 4D). For higher resolution and in order to identify a core myeloid signature, 100 FlowSOM clusters were run on all cells and $CD14^+$ myeloid cells were extracted. Clusters 8, 9, and 18 differed in some markers such as CD14, CD11c and PD-L1 expression but were still elevated in R over NR showing that they are a relatively homogenous cell population (Supplementary Figure 8).

Identification of a monocyte signature using CellCnn

FlowSOM allowed us to identify and characterize $CD14^+CD16b^-$HLA-DR^{hi} monocytes as being elevated in responders compared to non-responders prior to anti-PD-1 immunotherapy. To identify a core myeloid signature within $CD14^+CD16b^-$HLA-DR^{hi} cells that would allow us to predict responsiveness to anti-PD-1 immunotherapy without prior assumptions, we used the machine learning algorithm CellCnn, which is based on a representation learning approach using

convolutional neural networks and is designed to detect rare cell populations associated with disease status[22]. In a data driven way, CellCnn automatically "learns" combinations of markers ("filters", which do not need to correspond to known populations), whose presence or frequency discriminates between two groups. We ran CellCnn on all cells of the baseline samples with staining panel 3 and identified a discriminating cell population with a relative abundance of 4.8% +/- 2.0% (mean +/- standard deviation) in responders compared to 2.4% +/- 1.5% in non-responders (Supplementary Figure 9). Although the variability within each group was relatively large, we found the difference in abundance to be statistically significant (p-value < 0.01, see Supplementary Materials). In terms of marker expression, we found that this automatically detected population contained a core signature of $CD14^+$, $CD33^+$, HLA-DR^{hi}, ICAM-1^+, $CD64^+$, $CD141^+$, $CD86^+$, $CD11c^+$, $CD38^+$, PD-$L1^+$ and $CD11b^+$ monocytes (Supplementary Figure 9). Back projection of this cell population to the tSNE map, independently generated from all cells in panel 3, showed a striking overlap with the $CD14^+CD16^-$HLA-DR^{hi} cluster (Supplementary Figure 10).

In depth characterization of the myeloid compartment by RNA-seq

In a final approach, in order to characterize the identified myeloid cells in more depth, we performed RNA sequencing on sorted $CD14^+CD16^-$HLA-DR^{hi} cells from HD, NR and R at baseline. The most striking differences in gene-expression were observed between cancer patients and healthy donors. In particular, we found an enrichment in genes associated with metabolism, migration and inflammation in caner patients (Figure 4E). No immunosuppressive genes were found to be elevated in the circulating $CD14^+CD16^-$HLA-DR^{hi} cells of cancer patients as compared to healthy donors. Moreover, we found no significant difference in gene expression when comparing $CD14^+CD16^-$HLA-DR^{hi} cells of non-responders and responders, with the exception of CXCL2, which was marginally elevated in responders (Supplementary Figure 11). These data suggest that the frequency of circulating myeloid cells rather than gene-expression patterns or monocyte polarization correlates with responsiveness to anti-PD1 immunotherapy.

Validation of cellular immune signature by Citrus and conventional flow cytometry

As an independent validation of the computational results, we employed Citrus, which is a clustering-based supervised algorithm that identifies stratifying signatures, to compare the identified cell types and marker expression differences that could distinguish between non-responders and responders before therapy (Supplementary Figures 12 and 13). Citrus independently confirmed the lower frequency observed in the T cell compartment and the elevation of the myeloid compartment before therapy, as shown in panels 1 and 3.

To facilitate the translation of our observations into clinical practice, we designed a flow cytometry-based validation panel using a reduced number of markers. We selected a combination of markers that were significantly differentially expressed in Figures 1C and 4C and markers that define the cellular composition in the blood (Supplementary Figure 14). A blinded validation was performed on PBMCs from a second independent cohort of 31 melanoma patients containing 15 responders and 16 non-responders before anti-PD-1 therapy (Table 2).

Table 2 – Characteristics of melanoma patients and healthy donors used for the validation study.

		Before therapy
Healthy donors	N TOTAL	14
	Age in years – mean (range)	63.4 (46-91)
	Sex – male/female	7/7
Melanoma patients		
Responders	N TOTAL	15
	Age in years – mean (range)	58.9 (31-93)
	Sex – male/female	9/6
Non-responders	N TOTAL	16
	Age in years – mean (range)	61.9 (27-89)
	Sex – male/female	8/8

The data confirmed the lower frequency of T cells ($CD3^+$ $CD56^-$, p=1.67e-02) and the higher frequency of $CD14^+$ monocytes ($CD3^-CD19^-CD14^+CD16^-HLA\text{-}DR^+$, p=1.99e-06) before therapy in responders, as already shown by mass cytometry (Figure 4F). In order to visualize and assess the survival benefit conferred by a higher frequency of classical monocytes prior to treatment, we calculated the optimal cut-off point in monocytes frequency, which best stratifies responders and non-responders. The calculated cutoff of 19.38% was then used to compute a cumulative hazard function for the high and low monocyte frequency groups. The resulting plot shows a clear

difference in hazard ratios between patients who have a high frequency or a low frequency of classical monocytes at baseline. Our model thus indicates that a classical monocyte frequency higher than 19.38%, before anti-PD1 therapy initiation, is predictive of a better treatment response and patient survival (Figure 4G).

Cox regression identified immature granulocytes and measured monocytes to be associated with progression free survival

Finally, using a Cox proportional-hazards model, we assessed the prognostic value of 53 standard clinical parameters (Supplementary Figure 15) plus the frequency of classical monocytes (all measured at the baseline) with progression-free survival (PFS) in all the 51 patients used in this study. Multiple variables were significant in the univariate analysis (Supplementary Figure 16). There were no additional variables robustly associated with PFS in the multivariate analysis (including all factors with p-values < 0.05 from the univariate analysis), other than immature granulocytes and classical monocytes (Supplementary Figure 16B). The same 53 parameters were tested for association with response (NR versus R) using linear models (LM) for continuous parameters and generalized linear models (GLM) for the binary parameters and confirmed classical monocytes to be different (data not shown). This was an exhaustive analysis of all features that are routinely recorded in a standard clinical setting and confirms the relevance of our discovery that the measurement of classical monocyte frequencies could provide a simple yet powerful tool to clinical practice.

DISCUSSION

The successful therapeutic responses in patients with advanced melanoma encouraged the application of anti-PD-1 immunotherapy to several other cancers, such as non-small cell lung carcinoma (NSCLC), metastatic renal cell carcinoma, metastatic squamous NSCLC, Hodgkin`s lymphoma, advanced gastric cancer, advanced bladder cancer, head and neck cancer, and triple negative breast cancer[2,3,23,5-7,9,24,25]. Despite increasing overall survival in 33-40% of melanoma patients, anti-PD1 treatment is not effective in the majority of treated patients and results in disease progression at a median follow-up of 21 months in only 25% of patients[26,27]. Moreover, given the broadening of its application, we can anticipate that the rate of non-responding and relapsing patients to anti-PD-1 therapy will further increase. In this context, the identification of biomarkers allowing for the discrimination of responders and non responders before therapy initiation may tailor the application of this treatment only to those patients that are likely to benefit from it, while providing alternative treatments to the patients that are unlikely to show a response. In our study, by using single cell mass cytometry combined with clustering and regression analyses, we searched for differential immune signatures in responders versus non-responders before therapy. Besides a modest alteration of the lymphocyte compartment before therapy, i.e. lymphopenia of CD4 and CD8 T cells, γδT cells and a slight elevation of NKT cells, we could clearly show that classical $CD14^{+}CD16^{-}CD33^{+}HLA\text{-}DR^{hi}$ monocytes were the strongest predictor of responsiveness to anti-PD-1 immunotherapy.

The higher frequency of $CD14^{+}CD16^{-}CD33^{+}HLA\text{-}DR^{hi}$ classical monocytes in responders before therapy is striking. In recent years, the role of myeloid cells in cancer has been extensively debated and numerous studies have addressed the role of the so called myeloid derived suppressor cells, which have been shown to arise during chronic inflammation and cancer[28]. However, the phenotypic, morphological and functional heterogeneity of these cells generates confusion when investigating their roles in anti-cancer immune responses. It has been proposed that high frequencies of myeloid cells with immunosuppressive features, defined as $CD33^{+}CD11b^{+}HLA\text{-}DR^{lo/-}$, may lead to T cell dysfunction and failure to respond to immunotherapy. Accordingly, a reduction of suppressive myeloid cells correlated with an increase in the objective clinical responses and long-term survival[29-31]. Myeloid-associated

markers have been linked to poor clinical outcome[32,33]. In our study, we used clustering to define cell populations and found that the frequency of a cell population resembling $CD33^{low}CD11b^{+}HLA\text{-}DR^{lo}$ myeloid cells shows no differences between responders and non-responders and remains constant before and after therapy. In addition, in responding patients classical monocytes ($CD14^{+}CD16^{-}$) were highly activated as shown by increased ICAM-1 and HLA-DR levels. This suggests that monocytes may sustain the development of an effective anti-tumor immune response during anti PD-1 immunotherapy, similarly to what has been described for $CD14^{-}CD16^{+}$ monocytes during anti-CTLA-4 treatment[34]. Further support for a critical role of monocytes in anti-tumor immune responses comes from a study in which untreated melanoma patients with the highest tumor burden harbored dysregulated intermediate ($CD14^{+}CD16^{+}$) and non-classical monocytes ($CD14^{-}CD16^{+}$) characterized by a dramatic decrease of HLA-DR and inflammatory markers[35]. Further, the up-regulation of PD-L1 on the monocytes from responders before therapy could be a result of the higher activation status of these cells. It is well described that IFN-γ can induce the up-regulation of PD-1 and PD-L1 on T and myeloid cells, respectively[36,37].

In line with the notion that the presence of highly activated classical monocytes may be a prerequisite for a successful response during anti-PD-1 immunotherapy we reported higher frequencies of central memory T cells and NKT cells in circulation and a more activated ($CTLA\text{-}4^{+}$, $TNF\text{-}\alpha^{+}$, $PD\text{-}1^{+}$, $granzyme\text{-}B^{+}$ and $IL\text{-}2^{+}$) T cell compartment after therapy in responding patients. This is consistent with the observation by Wherry and colleagues that after 3 weeks of anti-PD-1 therapy T cell proliferation peaks but can still be observed after 12 weeks[20].

Given the shift of frequency from naïve to central memory T cells in responders before therapy and the increase in CTLA-4, IFN-γ, IL-17A, granzyme-B and PD-1 after therapy, our findings confirm that anti-PD-1 immunotherapy supports functionally activated T cells. This is in line with recent research showing that higher levels of CTLA-4 on intra-tumoral T cells correlated with better response to anti-PD-1 treatment and that resistance to anti-PD-1 immunotherapy was associated with defects in the pathways of antigen presentation and interferon-receptor signalling[10,36]. Indeed, besides being a regulator during T cell expansion, CTLA-4 is also a marker of activated T cells[38]. Further, enhanced NK T cell frequencies after immunotherapy

correlated with positive clinical responses in melanoma patients, while elevated frequencies of some γδT cell subsets following anti-CTLA4 treatment correlated with decreased clinical benefit[39,40]. Lastly, we found a consistent and significant reduction of T cells in the peripheral blood of responders compared to non-responders (Fig. 2C and D). This phenomenon may be due to their enhanced ability to migrate to the tumor site[41]. Indeed, we also found an up-regulation of CD11a in the $CD8^+$ T cell compartment of responder patients, which has been shown to be essential for migration to lymph nodes and distal sites [38,42]. Lastly, Th17 cells were recently demonstrated to be potent apoptosis-resistant anti-tumor effector cells[43,44].

The goal of this study was to interrogate the PBMC compartment for signatures that predict anti-PD-1 response. We observed that a reduction in T cell frequency and increase in myeloid cells -before therapy initiation- correspond with treatment response and overall survival. Further, the tendency of increased tumor infiltrating lymphocytes in R patients supports the notion that myeloid cell frequency increases when T cells move from the blood into the tumor, which is consistent with previous studies[10,41]. This phenomenon is - in all likelihood - the result of the increased (albeit insufficient) anti-tumor response in baseline patients, who are more likely become responders. Indeed, IFN-gamma produced by anti-tumor NK cells and T cells can trigger myeloid cell egress from the bone marrow[45,46]. In addition, IFN-gamma has been shown to enhance myeloid cell expansion[47]. Altogether, we provided evidence for a response-associated immune signature in metastatic melanoma patients during anti-PD-1 immunotherapy. In order to do this, we applied a recently-developed bioinformatics workflow[19]. The advantage of this workflow over existing methods, such as Citrus[48], is that we can compare multiple conditions (HD, R vs NR), account for sample pairing and adjust for batch effects, all in a single model. We are aware of the large variability between the two measurements in the discovery cohort, but, using our custom bioinformatic workflow, we were able to observe a significant difference in classical monocyte frequencies. Moreover, using traditional FACS analysis we could confirm this monocyte frequency difference in R vs NR patients in a second, blinded, independent cohort of patients undergoing immunotherapy.

Future studies entailing a systematic, prospective collection of paired blood and tumor samples should confirm these signatures in larger, multi-center cohorts of melanoma patients as well as in patients with other cancer types for which anti-PD-1 treatment

has been approved. A prediction signature could then be directly used in clinical practice to stratify patients prior to initiating immunotherapy. Our findings might help to further elucidate the mechanistic underpinnings of anti-PD-1 activity.

ONLINE METHODS

Patient Samples

Fifty-one cryopreserved peripheral blood mononuclear cells (PBMC) samples of melanoma patients (median: 84 days, range: 23-162 days, average: 87.3 days) were provided by the Department of Dermatology, University Hospital Zurich, Switzerland (see Table 1 and 2 and Supplementary Figure 17). From 20 of these patients, called the discovery cohort, samples before and about 12 weeks after anti-PD-1 immunotherapy initiation were used (N=40). Patients were treated with 3mg/kg Nivolumab every 2 weeks or 2mg/kg Pembrolizumab every 3 weeks for 12 weeks when their clinical status was assessed again. Response was defined as the patient's disease control rate (DCR) in the course of treatment. That is, the responder group comprises every patient who showed signs of clinical benefit within the first 15 weeks of treatment, which includes partial response (PR), complete response (CR), and stable disease (SD) thus better capturing "real-world-patients". The non-responder group included every patient who discontinued treatment due to disease progression or showed signs of progression within the first 15 weeks of treatment. Progression was defined as either a measurable increase in tumor size, new metastatic sites, or the need to treat the patient with a secondary treatment such as radiotherapy. The validation cohort was composed of 31 melanoma patients. Samples from the validation cohort were collected prior to anti-PD-1 therapy initiation.

Stimulations, stainings, and mass cytometry acquisition

PBMC stimulations, staining and acquisition by mass cytometry were performed as described previously[49]. Frozen PBMCs were used in this retrospective study to balance cohorts in terms of response and to reduce batch-effects through a unique bar-coding strategy. Data were stored using the Flow Repository[50] which can be accessed under: https://flowrepository.org/experiments/1124. Full methods are included in the Supplementary Materials.

Statistical Analysis

Data acquired by mass cytometry was normalized using the standalone MATLAB normalizer (Version 2013b)[51], marker expression was controlled in FlowJo (Version10.1r5) and patient samples were de-barcoded using Boolean gating. For further analysis we developed a customized R workflow in order to discover different biomarkers when comparing marker expression between responders and non-responders. The workflow is described in the Supplementary Materials and the R code can be accessed under: https://github.com/gosianow/carsten_cytof_code. Additional analyses to identify distinguishing cell subsets were done using CellCnn, see Supplementary Materials (code available under: https://github.com/lmweber/PD1_analysis_CellCnn).

Transcriptomic analysis

$CD14^{+}CD16^{-}HLA\text{-}DR^{hi}Lin^{-}$ (CD3, CD4, CD19, CD45RO) monocytes were sorted from frozen PBMC form blood samples from HD, R and NR at baseline. RNA was isolated using the RNA plus micro kit (Qiagen). We used the SMARTer Stranded total rna-seq pico kit (Clontech) for RNA preparations. Samples were sequenced on Illumina MySeq. Reads in FASTQ format from the 12 samples were quantified at the transcript level using Salmon[52] against an Ensembl catalog, aggregated to the gene level using tximport[53] and delivered to edgeR[54] for the differential expression analysis using the GLM functionality[55]. To determine differential expression, a (false discovery rate) FDR cutoff of 5% and minimum fold-change of 1.5 was used. Due to the gender bias in responders (R) versus non-responders (NR), 14 genes from the Y chromosome were removed before differential expression analysis.

Validation by flow cytometry

Validation of the CyTOF data was done with a combination of markers with significantly different expression from the initial discovery mass cytometry approach, and markers that defined the cellular composition in blood using flow cytometry (Supplementary Figure 9). A set of PBMCs was analyzed in a blinded fashion from a second, independent cohort of 31 melanoma patients containing 15 responders and 16 non-responders before anti-PD-1 therapy. The panel is described in the Supplementary Materials. At least 100`000 live cells were acquired using Diva

software on a Fortessa flow cytometer (BD) and analyzed using FlowJo software (TriStar). From FlowJo data, the frequencies of $CD3^+$ T cells and $CD14^+CD16^-HLA\text{-}DR^{hi}$ monocytes were extracted from the three groups (R, NR, HD). For statistical testing, we applied a generalized linear model (GLM) and cutpoint calculations as described in the Supplementary Materials.

References

1. Topalian, S. L., Drake, C. G. & Pardoll, D. M. Targeting the PD-1/B7-H1(PD-L1) pathway to activate anti-tumor immunity. *Curr. Opin. Immunol.* **24,** 207–212 (2012).
2. Topalian, S. L. *et al.* Safety, activity, and immune correlates of anti-PD-1 antibody in cancer. *N. Engl. J. Med.* **366,** 2443–2454 (2012).
3. Powles, T. *et al.* MPDL3280A (anti-PD-L1) treatment leads to clinical activity in metastatic bladder cancer. *Nature* **515,** 558–562 (2014).
4. Brahmer, J. *et al.* Nivolumab versus Docetaxel in Advanced Squamous-Cell Non-Small-Cell Lung Cancer. *N. Engl. J. Med.* **373,** 123–135 (2015).
5. Motzer, R. J. *et al.* Nivolumab versus Everolimus in Advanced Renal-Cell Carcinoma. *N. Engl. J. Med.* **373,** 1803–1813 (2015).
6. Rizvi, N. A. *et al.* Activity and safety of nivolumab, an anti-PD-1 immune checkpoint inhibitor, for patients with advanced, refractory squamous non-small-cell lung cancer (CheckMate 063): a phase 2, single-arm trial. *Lancet Oncol.* **16,** 257–265 (2015).
7. Ansell, S. M. *et al.* PD-1 blockade with nivolumab in relapsed or refractory Hodgkin's lymphoma. *N. Engl. J. Med.* **372,** 311–319 (2015).
8. Center for Drug EvaluationResearch. Approved Drugs - Hematology/Oncology (Cancer) Approvals & Safety Notifications. (2016).
9. Hamid, O. *et al.* Safety and tumor responses with lambrolizumab (anti-PD-1) in melanoma. *N. Engl. J. Med.* **369,** 134–144 (2013).
10. Daud, A. I. *et al.* Tumor immune profiling predicts response to anti-PD-1 therapy in human melanoma. *J. Clin. Invest.* **126,** 3447–3452 (2016).
11. Dronca, R. S. *et al.* T cell Bim levels reflect responses to anti-PD-1 cancer therapy. *JCI Insight* **1,** (2016).
12. Wistuba-Hamprecht, K. *et al.* Establishing High Dimensional Immune Signatures from Peripheral Blood via Mass Cytometry in a Discovery Cohort of Stage IV Melanoma Patients. *J. Immunol.* **198,** 927–936 (2017).
13. Mair, F. *et al.* The end of gating? An introduction to automated analysis of high dimensional cytometry data. *European Journal of Immunology* **46,** 34–43 (2016).
14. Pérez-Callejo, D., Romero, A., Provencio, M. & Torrente, M. Liquid biopsy based biomarkers in non-small cell lung cancer for diagnosis and treatment monitoring. *Transl Lung Cancer Res* **5,** 455–465 (2016).
15. Levine, J. H. *et al.* Data-Driven Phenotypic Dissection of AML Reveals Progenitor-like Cells that Correlate with Prognosis. *Cell* **162,** 184–197 (2015).
16. Van Gassen, S. *et al.* FlowSOM: Using self-organizing maps for visualization and interpretation of cytometry data. *Cytometry Part A* **87,** 636–645 (2015).
17. Weber, L. M. & Robinson, M. D. *Comparison of Clustering Methods for High-Dimensional Single-Cell Flow and Mass Cytometry Data*. (2016). doi:10.1101/047613
18. Maaten, L. V. D. & Hinton, G. Visualizing Data using t-SNE. *Journal of Machine Learning Research* **9,** 2579–2605 (2008).
19. Nowicka, M. *et al.* CyTOF workflow: differential discovery in high-throughput high-dimensional cytometry datasets. *F1000Research* **6,** 748 (2017).
20. Huang, A. C. *et al.* T-cell invigoration to tumour burden ratio associated with anti-PD-1 response. *Nature* **545,** 60–65 (2017).
21. Kamphorst, A. O. *et al.* Proliferation of PD-1+ CD8 T cells in peripheral blood after PD-1-targeted therapy in lung cancer patients. *Proc. Natl. Acad. Sci. U.S.A.* **114,** 4993–4998 (2017).
22. Arvaniti, E. & Claassen, M. Sensitive detection of rare disease-associated cell subsets via representation learning. (2016). doi:10.1101/046508
23. Brahmer, J. R. *et al.* Phase I study of single-agent anti-programmed death-1 (MDX-1106) in refractory solid tumors: safety, clinical activity, pharmacodynamics, and immunologic correlates. *J. Clin. Oncol.* **28,** 3167–3175 (2010).
24. Brahmer, J. R. *et al.* Safety and activity of anti-PD-L1 antibody in patients with advanced cancer. *N. Engl. J. Med.* **366,** 2455–2465 (2012).
25. Weber, J. S. *et al.* Nivolumab versus chemotherapy in patients with advanced melanoma who progressed after anti-CTLA-4 treatment (CheckMate 037): a randomised, controlled, open-label, phase 3 trial. *Lancet Oncol.* **16,** 375–384 (2015).
26. Robert, C. *et al.* Pembrolizumab versus Ipilimumab in Advanced Melanoma. *N. Engl. J. Med.* **372,** 2521–2532 (2015).
27. Ribas, A. *et al.* Association of Pembrolizumab With Tumor Response and Survival Among

Patients With Advanced Melanoma. *JAMA* **315,** 1600–1609 (2016).
28. Ostrand-Rosenberg, S. & Sinha, P. Myeloid-derived suppressor cells: linking inflammation and cancer. *J. Immunol.* **182,** 4499–4506 (2009).
29. Gebhardt, C. *et al.* Myeloid Cells and Related Chronic Inflammatory Factors as Novel Predictive Markers in Melanoma Treatment with Ipilimumab. *Clin. Cancer Res.* **21,** 5453–5459 (2015).
30. Meyer, C. *et al.* Frequencies of circulating MDSC correlate with clinical outcome of melanoma patients treated with ipilimumab. *Cancer Immunol. Immunother.* **63,** 247–257 (2014).
31. Sade-Feldman, M. *et al.* Clinical Significance of Circulating CD33+CD11b+HLA-DR- Myeloid Cells in Patients with Stage IV Melanoma Treated with Ipilimumab. *Clin. Cancer Res.* (2016). doi:10.1158/1078-0432.CCR-15-3104
32. Komohara, Y., Jinushi, M. & Takeya, M. Clinical significance of macrophage heterogeneity in human malignant tumors. *Cancer Sci.* **105,** 1–8 (2014).
33. Zhang, Q.-W. *et al.* Prognostic Significance of Tumor-Associated Macrophages in Solid Tumor: A Meta-Analysis of the Literature. *PLoS ONE* **7,** e50946 (2012).
34. Romano, E. *et al.* Ipilimumab-dependent cell-mediated cytotoxicity of regulatory T cells ex vivo by nonclassical monocytes in melanoma patients. *Proc. Natl. Acad. Sci. U.S.A.* **112,** 6140–6145 (2015).
35. Chavan, R. *et al.* Untreated stage IV melanoma patients exhibit abnormal monocyte phenotypes and decreased functional capacity. *Cancer Immunology Research* **2,** 241–248 (2014).
36. Zaretsky, J. M. *et al.* Mutations Associated with Acquired Resistance to PD-1 Blockade in Melanoma. *N. Engl. J. Med.* **375,** 819–829 (2016).
37. Bellucci, R. *et al.* Interferon-γ-induced activation of JAK1 and JAK2 suppresses tumor cell susceptibility to NK cells through upregulation of PD-L1 expression. *Oncoimmunology* **4,** e1008824 (2015).
38. Herbst, R. S. *et al.* Predictive correlates of response to the anti-PD-L1 antibody MPDL3280A in cancer patients. *Nature* **515,** 563–567 (2014).
39. Ibarrondo, F. J. *et al.* Natural killer T cells in advanced melanoma patients treated with tremelimumab. *PLoS ONE* **8,** e76829 (2013).
40. Wistuba-Hamprecht, K. *et al.* Proportions of blood-borne Vδ1+ and Vδ2+ T-cells are associated with overall survival of melanoma patients treated with ipilimumab. *Eur. J. Cancer* **64,** 116–126 (2016).
41. Kluger, H. M. *et al.* Characterization of PD-L1 Expression and Associated T-cell Infiltrates in Metastatic Melanoma Samples from Variable Anatomic Sites. *Clin. Cancer Res.* **21,** 3052–3060 (2015).
42. Andrian, von, U. H. & Mempel, T. R. Homing and cellular traffic in lymph nodes. *Nat. Rev. Immunol.* **3,** 867–878 (2003).
43. Bowers, J. S. *et al.* Th17 cells are refractory to senescence and retain robust antitumor activity after long-term ex vivo expansion. *JCI Insight* **2,** e90772 (2017).
44. Neitzke, D. J. *et al.* Murine Th17 cells utilize IL-2 receptor gamma chain cytokines but are resistant to cytokine withdrawal-induced apoptosis. *Cancer Immunol. Immunother.* **4,** 128–15 (2017).
45. Takizawa, H., Regoes, R. R., Boddupalli, C. S., Bonhoeffer, S. & Manz, M. G. Dynamic variation in cycling of hematopoietic stem cells in steady state and inflammation. *J. Exp. Med.* **208,** 273–284 (2011).
46. Nagai, Y. *et al.* Toll-like Receptors on Hematopoietic Progenitor Cells Stimulate Innate Immune System Replenishment. *Immunity* **24,** 801–812 (2006).
47. Caux, C., Moreau, I., Saeland, S. & Banchereau, J. Interferon-gamma enhances factor-dependent myeloid proliferation of human CD34+ hematopoietic progenitor cells. *Blood* **79,** 2628–2635 (1992).
48. Bruggner, R. V., Bodenmiller, B., Dill, D. L., Tibshirani, R. J. & Nolan, G. P. Automated identification of stratifying signatures in cellular subpopulations. *Proc. Natl. Acad. Sci. U.S.A.* **111,** E2770–7 (2014).
49. Hartmann, F. J. *et al.* High-dimensional single-cell analysis reveals the immune signature of narcolepsy. *J. Exp. Med.* **213,** 2621–2633 (2016).
50. Spidlen, J. & Brinkman, R. R. Use FlowRepository to share your clinical data upon study publication. *Cytometry B Clin Cytom* (2016). doi:10.1002/cyto.b.21393
51. Finck, R. *et al.* Normalization of mass cytometry data with bead standards. *Cytometry Part A* **83,** 483–494 (2013).

52. Patro, R., Duggal, G., Love, M. I., Irizarry, R. A. & Kingsford, C. Salmon provides fast and bias-aware quantification of transcript expression. *Nat. Methods* **14,** 417–419 (2017).
53. Soneson, C., Love, M. I. & Robinson, M. D. Differential analyses for RNA-seq: transcript-level estimates improve gene-level inferences. *F1000Research* **4,** 1521 (2015).
54. Robinson, M. D., McCarthy, D. J. & Smyth, G. K. edgeR: a Bioconductor package for differential expression analysis of digital gene expression data. *Bioinformatics* **26,** 139–140 (2010).
55. McCarthy, D. J., Chen, Y. & Smyth, G. K. Differential expression analysis of multifactor RNA-Seq experiments with respect to biological variation. *Nucleic Acids Research* **40,** 4288–4297 (2012).

Acknowledgements

We thank Drs. V. Tosevski and T.M. Brodie from the mass cytometry core facility, University Zurich, Alice Langer from Dermatology Department, University Zurich and Dr. C. Beisel and K. Eschbach from the Genomics Facility, ETH Basel for excellent technical assistance and Drs. Bithi Chatterjee and Cornelia Gujer from the Department of Experimental Immunology, University Zurich, Alix Zollinger from the Swiss Institute of Bioinformatics, Lausanne and all members of the COST Action BM1404 MyeEUNITER (www.mye-euniter.edu) for discussion. This work received funding from the University Research Priority Program (URPP) in Translational Cancer Research, the Swiss National Science Foundation (310030_146130 and 316030_150768 to B.B.) and the European Union FP7 project ATECT (BB).

Competing Financial Interest

The authors declare no competing financial interest.

Author's contributions

C.K., M.P.L. and B.B. conceived the study and analyzed data.

C.K., S.G. and B.B. designed and performed the experiments.

F.H. and S.G. assisted with the experiments.

S.S., R.D. and M.P.L. provided clinical samples and performed statistical analysis of clinical parameters. R.D. and M.P.L. analyzed histology.

M.N., L.M.W. and M.D.R. provided analysis algorithms and analyzed data.

C.K., S.G. wrote and M.P.L., M.D.R. and B.B. edited the manuscript.

All authors read and gave final approval to submit the manuscript.

FIGURES

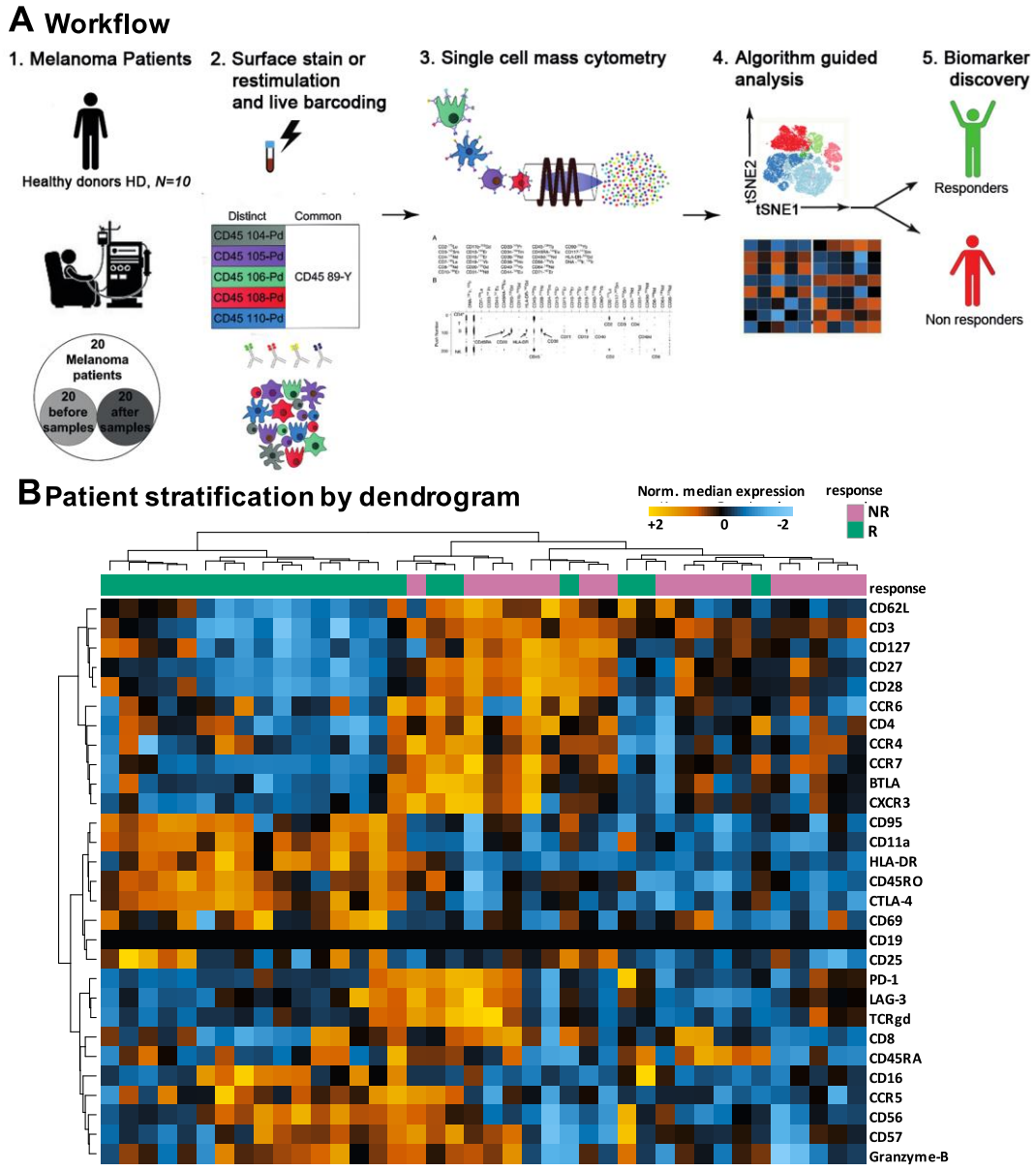

Figure 1. Stratification of responders and non-responders and identification of differences in immune cell populations using mass cytometry. (**A**) Experimental setup for the processing of frozen PBMC from matched samples before and after PD-1 immunotherapy from 20 melanoma patients using metal-labeled antibodies and acquisition by mass cytometry. (**B**) Heatmap of median arcsinh-transformed marker expression normalized per batch to mean of zero and standard deviation of one. Orange indicates relative over-expression, blue under-expression. The median expression is calculated on $CD45^+$ single live cells of thawed patient PBMCs. The dendrograms for markers (rows) and samples (columns) were constructed with hierarchical clustering (Euclidean distance, Ward linkage). Bars on top of the heatmap represent individual samples from responders (green) and non-responders (pink). Each column represents one patient sample from one time point (no. patients=20, no. samples=40).

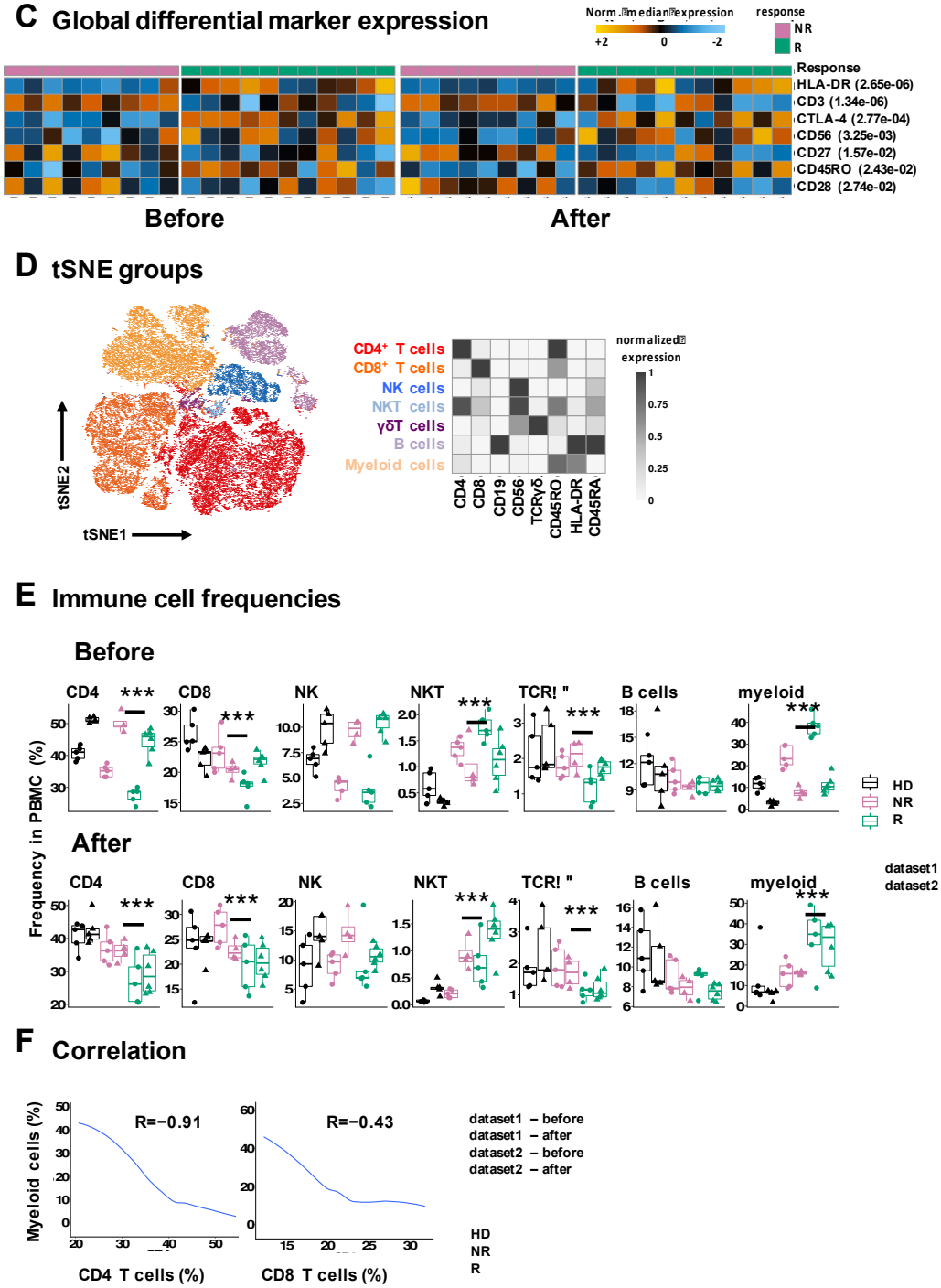

Figure 1 (continued). Stratification of responders and non-responders and identification of differences in immune cell populations using mass cytometry.

(**C**) Heatmap of median arcsinh-transformed marker expression normalized per batch to mean of zero and standard deviation of one for markers that are significantly (adjusted p-value < 0.05) differentially expressed between responders and non-responders before and 12 weeks after therapy initiation, in pre-processed live single cells. Colored bars on top of the heatmap represent individual samples from responders (green) and non-responders (pink). Numbers in brackets indicate adjusted p-values. (**D**)

tSNE visualization of 45`000 merged events from non-responders (NR), responders (R), and healthy donors (HD) from dataset 1. Cells are colored according to the cluster they were assigned to using the FlowSOM algorithm and manual annotation. The heatmap represents the median arcsinh-transformed marker expression normalized to 0-1 range of respective markers within the 7 cellular clusters from dataset 1 and was used to annotate clusters. (**E**) Direct comparison of cluster frequencies in healthy donors (HD, black), non-responders (NR, pink) and responders (R, green) in dataset 1 and 2. Asterisks indicate the significance level of differences in cell frequencies between NR and R before and after treatment (adjusted p-value < 0.01***). (**F**) Relationship between CD4 or CD8 T cell frequency and myeloid cell frequency. R indicates Spearman correlation between these quantities.

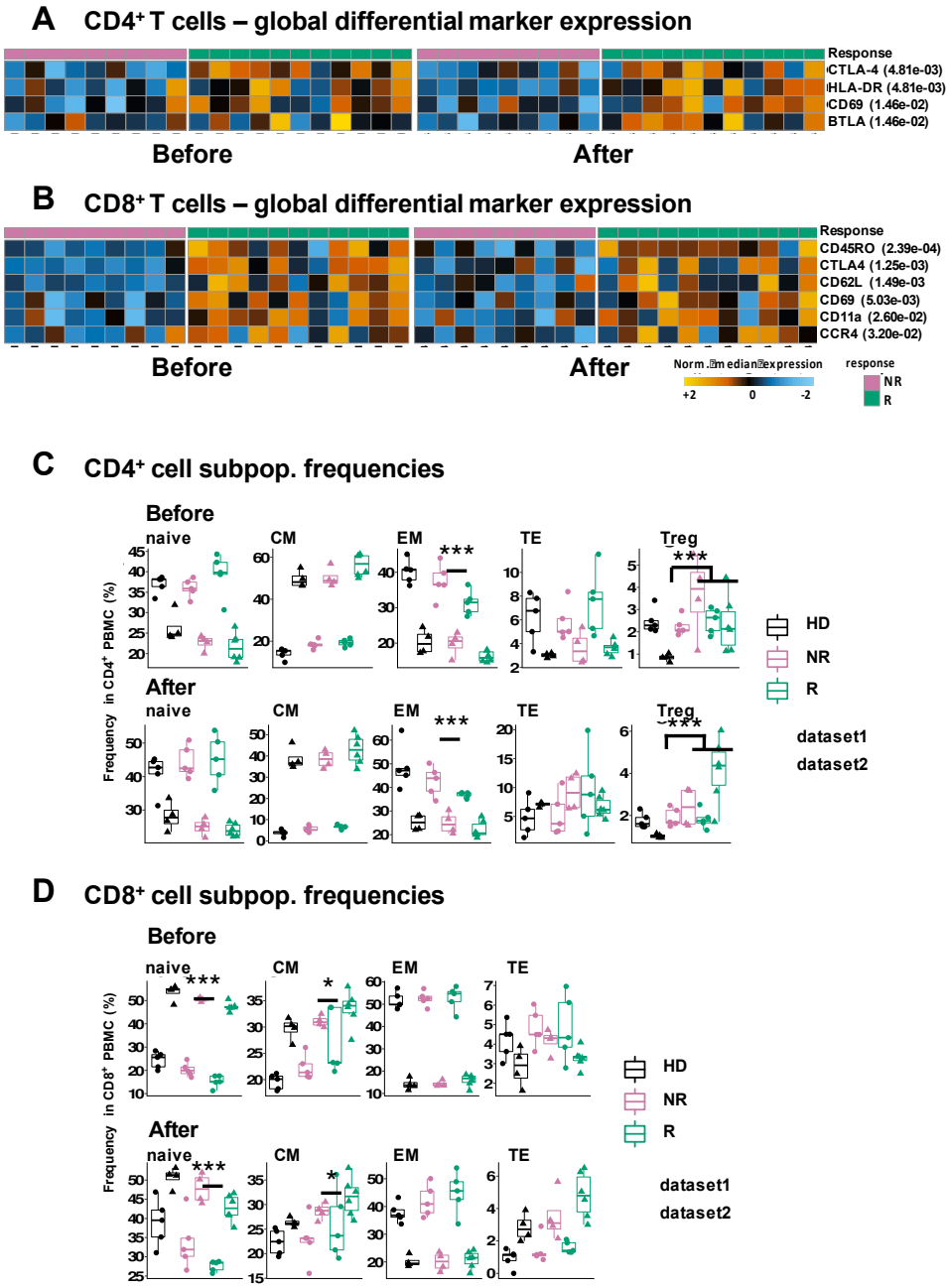

Figure 2. Differences in T cell activation status and in the frequency of the T cell subpopulations before and after 12 weeks of therapy in responders and non-responders. (**A, B**) Heatmap of per batch normalized (mean of zero and standard deviation of one) median marker expression for markers that are significantly (adjusted p-value < 0.05) differentially expressed between responders (green bar on top) and non-responders (pink bar on top) before and after therapy in $CD4^+$ T cells and $CD8^+$ T cells. Numbers in brackets show adjusted p-values. (**C**, **D**) FlowSOM was used to generate indicated T cell subpopulations and resultant cluster frequencies are plotted as in Figure 1E. Asterisks indicate the significance level of differences in cell frequencies between NR and R before and after treatment, except for Tregs, where the difference between HD and cancer patients (R and NR) was tested (adjusted p-value < 0.01***, < 0.1*).

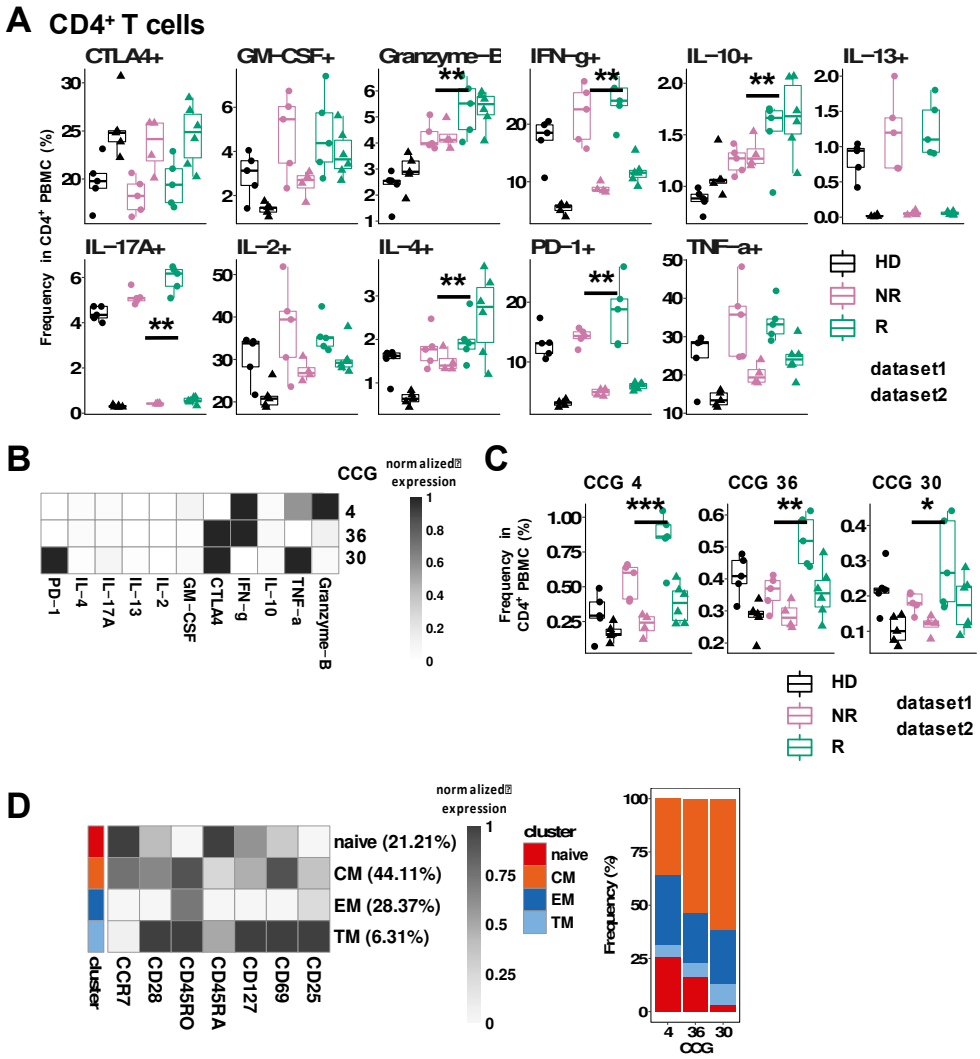

Figure 3. Increased activation in CD4⁺ or CD8⁺ T cells after immunotherapy start in responders.

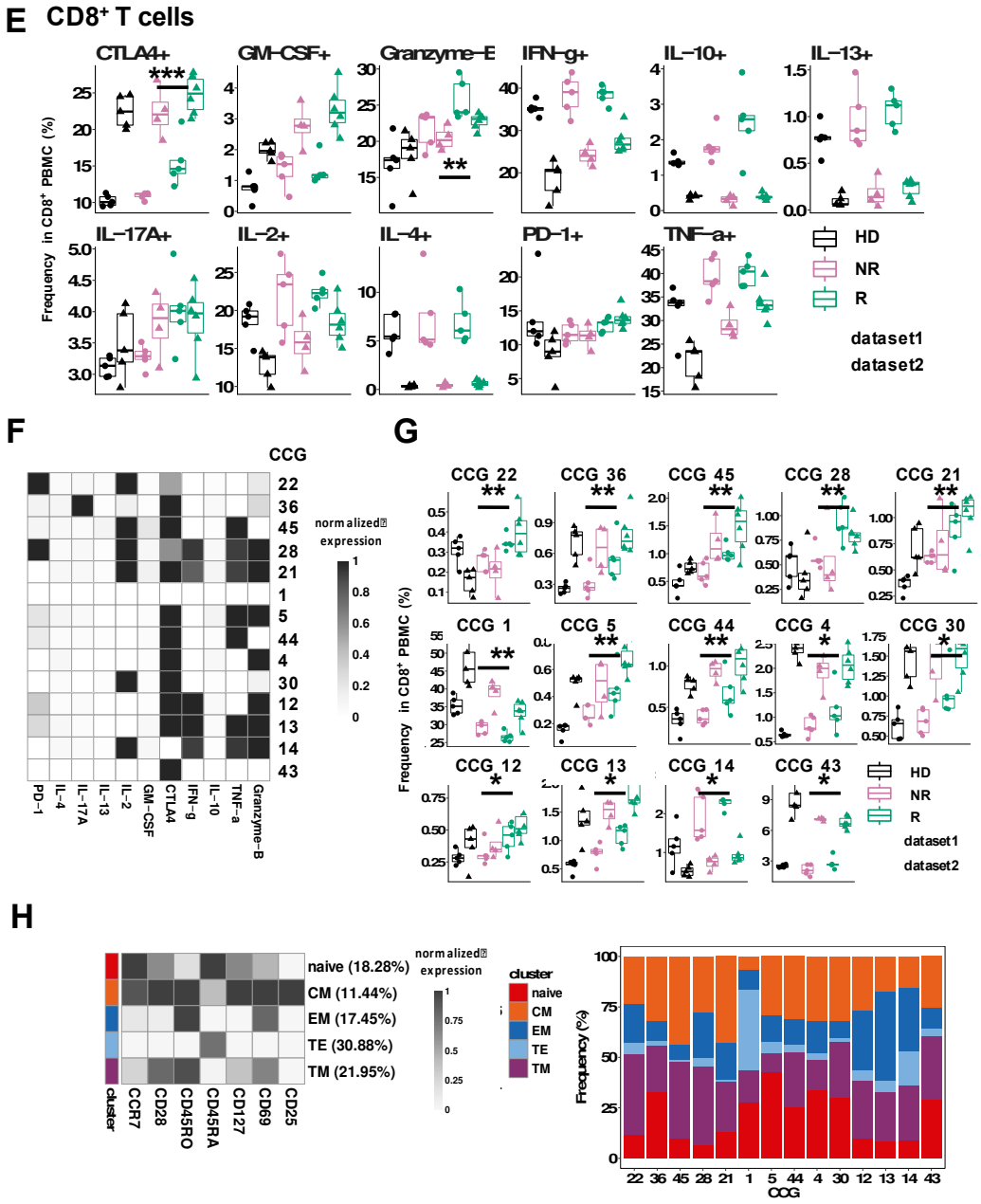

Figure 3 (continued). Increased activation in CD4⁺ or CD8⁺ T cells after immunotherapy start in responders. CD4⁺ and CD8⁺ T cells after therapy were polyclonally activated with PMA/Ionomycin. Frequencies of PD-1, CTLA-4, and cytokines in (**A, E**) CD4⁺ T cells and CD8⁺ T cells in responders (green) and non-responders (pink) were compared. Healthy subjects (black) served as controls. Asterisks indicate the significance level of differences in cell frequencies between NR and R after treatment (adjusted p-value < 0.01***, < 0.05**, < 0.1*) (**B, F**) A matrix combining all cytokine positive cells into cytokine combination groups (CCGs) for CD4⁺ T cells and CD8⁺ T cells was created and cells were sorted into this matrix using FlowSOM. Shown are the significantly different CCGs after comparing responders to non-responders. (**C**, **G**) Shown are frequencies of significantly different CCGs between responders and non-responders from that matrix. (**D, H**) The phenotypic composition of the significantly different CCGs for CD4⁺ T cells and CD8⁺ T cells (right panel). Phenotypes were derived from heatmaps shown in the left panel.

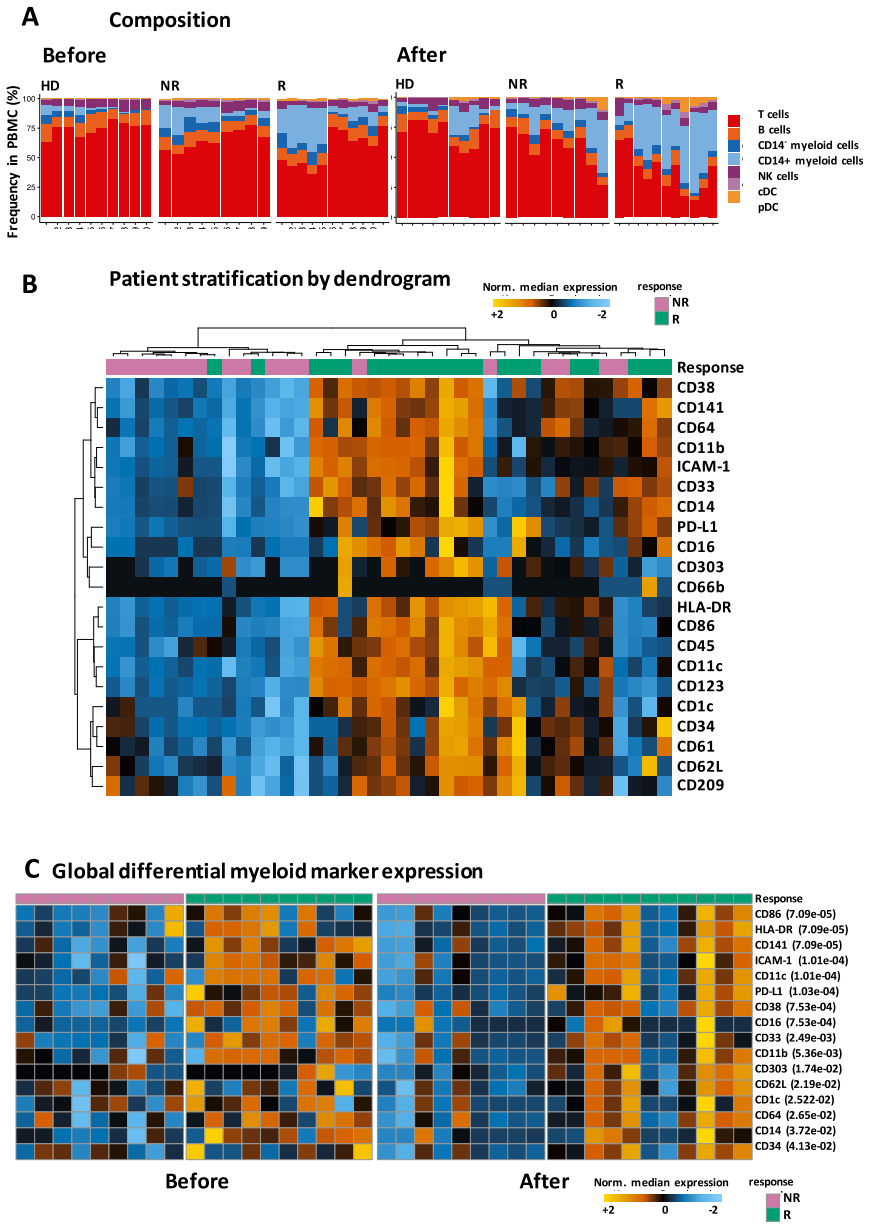

Figure 4. Patient stratification based on myeloid cell markers and expansion and enhanced activation of classical monocytes in responders. (**A**) Comparison of sample composition in healthy donors (HD) non-responders (NR) and responders (R) before and after anti-PD-1 therapy. (**B**) Heatmap of normalized median marker expression with dendrograms for markers (rows) and samples (columns) constructed, as in Figure 1B, for myeloid markers. Bars on top of the heatmap represent individual samples from responders (green) and non-responders (pink) from the two time points (no. patients=20, no. samples=39 - one baseline sample with a cell count < 50 was excluded from the further analysis. (**C**) Heatmap of normalized median marker expression for markers that are significantly (adjusted p-value < 0.05) differentially expressed between responders and non-responders before and 12 weeks after therapy initiation, as in Figure 1C, in the myeloid compartment ($CD3^{-}CD19^{-}$). Bars on top of the heatmaps represent individual samples from responders (green) versus non-responders (pink). Numbers in brackets show adjusted p-values.

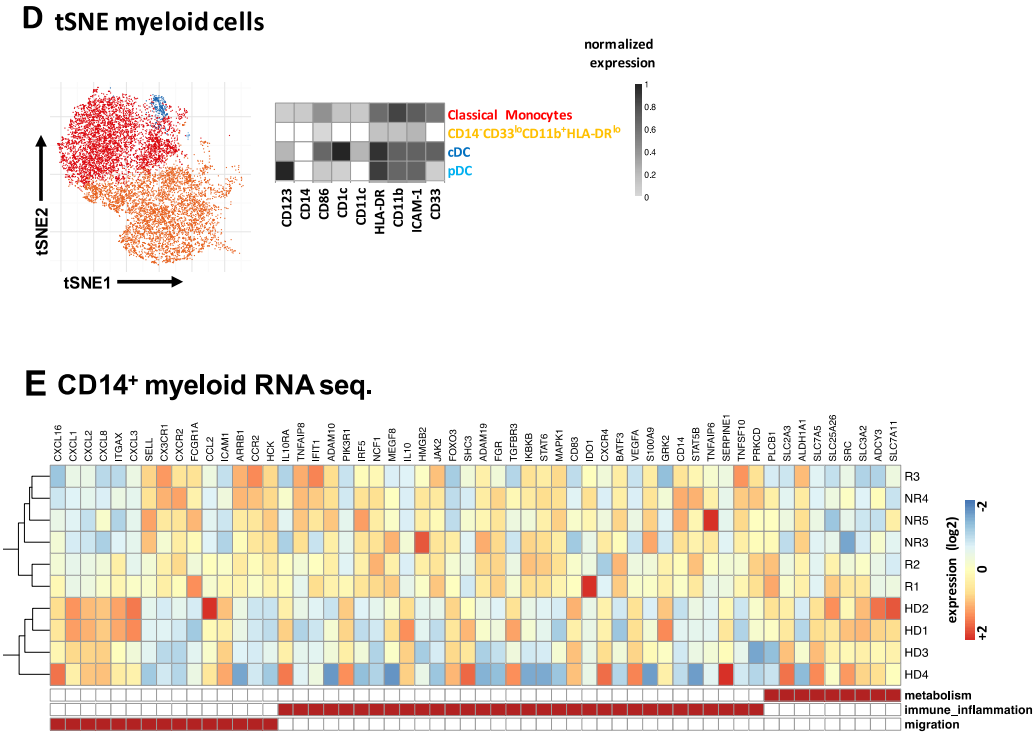

Figure 4 (continued). Patient stratification based on myeloid cell markers and expansion and enhanced activation of classical monocytes in responders. (**D**) tSNE visualization of FlowSOM-generated myeloid clusters ($CD3^{-}CD19^{-}$) in merged data from non-responders (NR), responders (R) and health donors (HD), as in Figure 1D. $CD7^{+}$ and $CD56^{+}$ cells were excluded from analysis. The heatmap on the right represents the expression of respective markers within the cellular clusters. (**E**) RNA sequencing analysis of $CD14^{+}CD16^{-}HLA\text{-}DR^{hi}$ monocytes sorted form HD, R, and NR before therapy displaying a heatmap of 56 significantly different genes when comparing HD to cancer patients (R and NR). Expression values were quantified with Salmon and represented as a fold-change relative to the median gene expression. Differential expression was determined using edgeR. The three columns on the left sort the genes according to their function (migration, inflammation and metabolism).

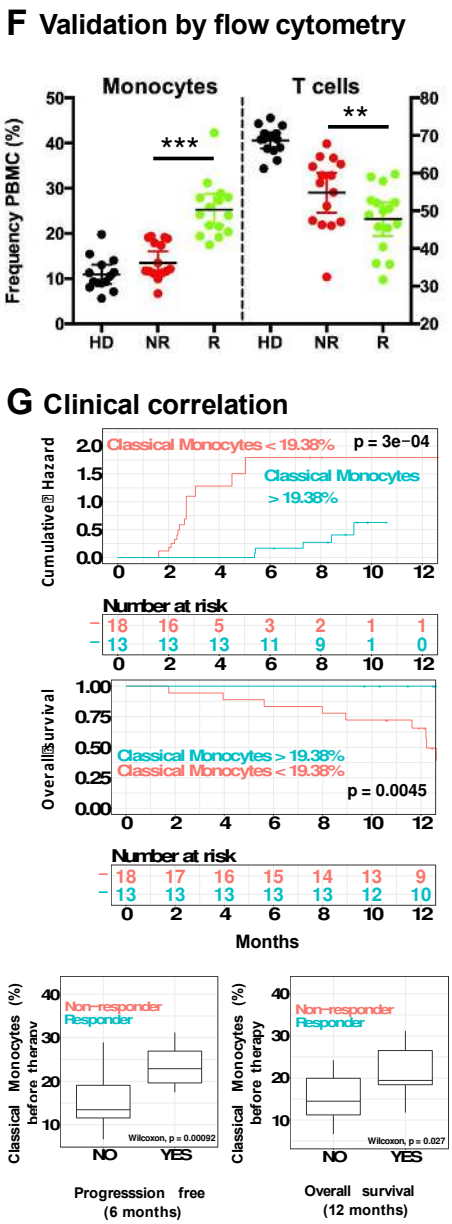

Figure 4 (continued). Patient stratification based on myeloid cell markers and expansion; enhanced activation of classical monocytes in responders. (**F**) Validation of results on a second independent cohort of 31 patients using flow cytometry and CD3, CD4, CD11b, CD14, CD19, CD16, CD33, CD56, HLA-DR markers (HD black, NR red, R green). (**G**) Cumulative hazard and overall survival in patients with monocyte frequencies above (blue) and below (red) 19.38% over time (months). Shows p-value of log-rank test. The box plots represent monocyte frequency at baseline against progression free survival (PFS) at 6 months and overall survival (OS) at 12 months in non-responders (red) and responders (blue). Wilcoxon test was used to calculate the displayed p-value.